"RESEARCH PROGRAM IN PARTICLE PHYSICS"

Progress Report

January 1, 1992 – December 1992

E. C. G. Sudarshan, Duane A. Dicus, Jack L. Ritchie, and Karol Lang

Center for Particle Theory
University of Texas
Austin, Texas 78712

July 1992

MASTER

DISTRIBUTION OF THIS DOCUMENT IS UNLIMITED

Preface

This progress report includes three tasks—one theoretical for which Dicus and Sudarshan are the principal investigators, and two other experimental for which Ritchie and Lang are the principal investigators. Accordingly it consists of three separate and complete parts, as can be seen from the Table of Contents on the next page.

Table of Contents

Progress Report of Task C -- Experimental

Progress Report

of

Task A

Theoretical

1 Introduction

This progress report of the Center for Particle Physics of the University of Texas at Austin reviews the work done over the past year and is part of the renewal proposal for the period from January 1, 1993 through December 31, 1993.

The senior academic staff of the Center for Particle Physics (Chiu, Dicus, Ne'eman and Sudarshan) has remained the same. Professor Gleeson and Professor Bohm are also members of the Center but were not part of this grant and all of their support came from other sources. The contribution to the contract research of Bohm and Gleeson is a contribution by the University and is not reviewed here. Professor Ne'eman was in residence for parts of the Fall semester and for a short period in the spring. The Center also has five members who are experimentalists; Jack Ritchie and Karol Lang, whose progress reports form another part of this document, Peter Riley and Jerry Hoffmann who have separate funding, and Roy Schwitters who is on leave as Director of the SSC. The research associate has been Dr. Debra Karatas. Some of the work reviewed here was by graduate students. Of these, José Pecina-Cruz (Ne'eman) completed his dissertation. Professor G. Bhamathi of Madras University spent the entire academic year visiting the Center. Professors Louis J. Boya and José.Gracia-Bondia of the University of Zaragoza (Spain), Dr. P. Morley of QED Research, Inc., and Dr. T. Imbo of Harvard University spent several months here. Visitors for shorter periods of time (weeks rather than months) were Scott Willenbrock (Brookhaven), S. Nandi (Oklahoma State), X. Tata (Hawaii), Tom Rizzo (Iowa State University), JoAnne Hewett (Argonne National Laboratory), Howie Baer (Florida State), Roberto Vega (SLAC), and Vic Teplitz (SMU). All the visitors collaborated with members of the Center and many wrote papers while here which are reviewed in this report. The staff supported by this grant have also benefited from collaborations with many people outside the University as indicated in the following report.

2 Research Report

2.1 Quantum Gravity and Mathematical Physics

QCD. Yuval Ne'eman was able to provide an exact derivation of his "Pseudo-Gravity" approximation, for the irreducible representation (IR) region of QCD. The Color-$SU(3)$ gauge transformations, when taken between IR region S-matrix elements for the pseudo-metric $G_{\mu\nu} = B_\mu^i B_{i\nu}$ is the gluon field (i is a Color $SU(3)$ index, μ a spacetime index) mimic the transformations of the metric tensor under (pseudo-) diffeomorphisms. The exchange of this pseudo-metric provides a long-range contribution resembling Gravity. The precise analogy is between QCD in its IR region and Gravity in its high-energy quantum region. The theory explains the emergence of the Arima-Iachello Interacting Boson Model in nuclei. In hadrons, it explains why the Quantum String, a theory of Gravity, does also provide a viable model for some of the features of Strong Interactions (Dual Models) and why suggestions as the Isham-Salam-Stratgdee Strong Gravity (in the seventies) also provided plausible results. With Dj. Sijacki, Y. Ne'eman was also able to show that pseudo-gravity dynamics predict the $M^2 \sim J$ behavior of hadron Regge trajectories.

$SU(2/1)$ and Superconnections. The Internal Superunification model based on $SU(2/1)$, which Y. Ne'eman introduced in 1979, predicts a mass for the Higgs field around 170 GeV. Y. Ne'eman has now produced a new chiral alternative interpretation of the basic representations fitting quarks and leptons. However, this interpretation would require a fermionic Higgs field. Y. Ne'eman's previous and preferred interpretation of the particle representations fits the geometric theory of superconnections (Quillen, Bott, etc.) which he independently developed (with J. Thierry-Mieg) in 1982. The formalism has now been further developed. Y. Ne'eman has also started an investigation of dynamical effects, using one-loop estimates.

Affine Gravity. Theories of Quantum Gravity based on Spontaneous Symmetry Breakdown of a gauged $SL(4, R)$ (such as the one developed by Y. Ne'eman with Dj. Sijacki and with C.Y. Lee) require the primordial particle Hilbert space to be given in terms of the Unitary Irreducible Representations ("unirreps") of the Special Affine Group $SA(4, R)$. Such representations would also be useful for a description of particles in curved space and for the above hadronic pseudo-gravity picture, etc. With J. Pecina-Cruz, Y. Ne'eman has investigated the Casimir invariant of $SA(n, R)$ and provided a classification of the unirreps.

An important physical result is that for the three above-mentioned physical situations, the Casimir vanishes and there is no kinematical constraint on the corresponding Regge trajectories, only the dynamical.

Studying the Casimir invariants has led Y. Ne'eman and J. Pecina-Cruz to develop general algorithms for such calculations. The method has been tried on a set of solvable algebras.

Ne'eman and Pecina-Cruz calculated the invariants for a Quantum Gauge Theory of Gravity based in the group $SA(4, R)$ (gauge theories of gravity based in the $GL(4, R)$ group do not contain elementary particles).[1] With them they constructed the unitary irreducible representations for this group and for its double covering group $\overline{SA}(4, R)$. The spectrum of the Casimir (invariant polynomial)of $SA(4, R)$ and its double covering group was found. From the spectrum of $SA(4, R)$ and its unitary irreducible representations we concluded that in this theory, which contains the Strong Interaction Force, there are not kinematical constrains on mass-spin relations.[2]

They also developed an algorithm to calculate the invariants for any Lie algebra which had been searched for long time.[4] The algorithm was applied to calculate the invariants for the group $SA(n, R)$ and the solvable Lie algebras of dimension six, which were unknown until this.[3]

2.2 Phenomenology

2.2.1 High Energy Phenomenology

Searches for the electroweak standard model Higgs boson H^0 at proposed high-energy colliders will include the mass region $m_H \gg 2m_Z$, where the H^0 decays are dominated by $H^0 \to W_L^+ W_L^-$ and $H^0 \to Z_L^0 Z_L^0$. The strength of the H^0 couplings to the longitudinal vector bosons $W_L^\pm$ and Z_L^0 depends on m_H/m_W and consequently scattering processes such as $W_L^+ W_L^- \to W_L^+ W_L^-$ can violate the unitary bound at the Born level for sufficiently large m_H as was first shown by Dicus and Mathur. By including one-loop corrections to the Born amplitudes, one finds that the perturbative amplitudes violate unitarity for $m_H \gtrsim 1.0 - 1.2$ TeV. In this range of m_H, the Higgs sector becomes strongly interacting. Consequently, the prediction of, say, $W_L^+ W_L^-$ pair production by W-fusion at pp colliders is very uncertain for $m_H \gtrsim 1.2$ TeV.

In order to get some sense of how increasing m_H beyond the perturbative regime might affect the gauge boson scattering amplitudes, Dicus and W. W. Repko of Michigan State

3

University have studied the $W_L^+ W_L^- - Z_L^0 Z_L^0$ system by unitarizing the s-wave amplitudes using the K-matrix and Padé approaches. For $m_H \gtrsim 10$ TeV, the K-matrix amplitudes are featureless in the invariant mass region 500 GeV $\lesssim m_V V \lesssim$ 2000 GeV. In this invariant mass region, the Padé amplitudes develop a $J = 0$ low-mass resonance, which is narrower than an elementary Higgs of the same mass. Now Dicus and Repko have used unitarized versions of the $W_L^+ W_L^- \to W_L^+ W_L^-$ and the $W_L^+ W_L^- \to Z_L^0 Z_L^0$ scattering amplitudes to explore the signature of this lower mass resonance in the invariant mass distributions for the processes $pp \to W_L^+ W_L^- X$ and $pp \to Z_L^0 Z_L^0 X$ at collider energies appropriate to the Superconducting Super Collider (SSC) and the Large Hadron Collider (LHC). In particular, if the [1,1] Padé approximant accurately reflects Nature's unitarized amplitude, can we tell the difference between the narrower resonance which occurs at $\sqrt{s} \sim 1$ TeV if $m_H \gtrsim 10$ TeV, and the broader resonance which occurs at $\sqrt{s} = m_H$ if $m_H \lesssim 1$ TeV, at the SSC or LHC?

In DOE-ER40200-258, Dicus and Repko give an explicit answer to this question. For example, if we assume a $10^4 pb^{-1}$ luminosity per year at the SSC, then a 10 GeV bin centered at 800 GeV would contain a background from the $q\bar{q} \to W^+ W^-$ process of 507 events per year for a rapidity cut $\eta_C = 2.5$. If m_H is 50 TeV, the Padé resonance would add to this to give a total of 585 $W_L^+ W_L^-$ events per year; if m_H is 950 GeV the total number of events is 619. This difference of 34 events should allow the determination of m_H. If the rapidity of each W is restricted to 1.0, the corresponding numbers are 40 events per year from the background and a total of 65 or 75 events for m_H equal to 50 TeV or 950 GeV. Thus, although the cross sections are down by a factor of 10, the difference between the high and low values of m_H is still striking. For the LHC, with a luminosity of $10^5 pb^{-1}$ per year, the difference for $\eta_C = 2.5$ is only 40 events out of a total of 2300. Similar results hold for ZZ production.

Dicus and Repko have also considered higher-order partial waves in $W_L^+ W_L^- \to W_L^+ W_L^-$ to determine if the [1,1] Padé approximant predicts resonances for $J > 0$, and, if so, the energies of these resonances and the relation between these energies and the Higgs mass m_H. It is expected, by analogy to pions with an elementary sigma particle, that these resonances will exist, and as shown in DOE-ER40200-267, they do.

They have studied the p-wave resonance determining its position and width for a broad range of possible values of the Higgs mass parameter m_H. They have also calculated the production cross section in pp collisions and find that the resonance should be observable if m_H is larger than 1 TeV up to an m_H value somewhere above 5 TeV. This region of m_H corresponds to a resonance position between 2.6 and 3.2 TeV.

4

It was suggested by Chanowitz and Golden that the enhancement in vector boson (VB) scattering due to their strong interactions from a heavy Higgs would be most apparent in the scattering of like-sign, longitudinally polarized W's: $W_L^\pm W_L^\pm \to W_L^\pm W_L^\pm$; the impetus for this is that compared to the other VB scattering channels the like-sign channel has intrinsically the smallest background level. Unfortunately, it was found by Dicus and Roberto Vega (SLAC) that the Standard Model (SM) yield of like-sign transversely polarized W-pairs ($W_T^\pm W_T^\pm$) would overwhelm any enhancement in the longitudinal mode scattering. To detect any longitudinal enhancement it seemed necessary to measure the polarizations of the W^+-pairs. Of course, this is not possible since charge determination of the W-pairs limits us to the purely leptonic decay modes. The only viable alternative is to find ways of suppressing the yield of like-sign W_T-pairs while retaining the signal for the like-sign W_L-pairs. Some work has been done along lines by several sets of authors including Dicus, Vega, and Jack Gunion (U. C. Davis). Now Dicus, Gunion, Vega and Lynne Orr (U. C. Davis) have explored in depth several techniques for detecting the l^+l^+ mass spectrum coming from W^+W^+ scattering. They demonstrate that anti-tagging against energetic centrally produced jets must be combined either with their earlier-proposed cut requiring single-jet tagging on the minimum jet-lepton invariant mass or with a cut on the isolation of the leptons in order to adequately suppress all backgrounds. In particular, they identify cuts that are sufficient to suppress the $t\bar{t}$-induced background below the level of the signal. Effects due to production of an extra gluon in association with the $t\bar{t}$ are included. Sensitivity to distribution functions and scale choices are explored. Event rates at the LHC, SSC and Eloisatron energies are given. Use of the isolation requirement along with staged implementation of the other cuts is proposed as a means for verifying the Standard Model expectation for the W^+W^+ spectrum in the case where the Higgs boson is light. Applicability of the proposed cut procedures to the purely leptonic decay modes of the W^+W^-, ZZ and $W^\pm Z$ channels are outlined. All this is given in DOE-ER40200-263.

Some time ago Weinberg argued that in the leading order in $1/N$, where N is the number of colors, the axial vector coupling of the constituent quark is equal to one and its anomalous magnetic moment is zero. This justifies the usual treatments of the constituent quark and bag models, where the quark is treated as a bare Dirac particle, provided the corrections in $1/N$ are shown to be small, especially for the magnetic moments. More recently Weinberg has given an estimate of the corrections of order $1/N$ to the axial vector coupling of the constituent quark. His calculation was done using the chiral quark model Lagrangian in the chiral limit and the limit of large number of colors. The essential input

was the analogue of the famous Adler-Weisberger sum rule for pion-quark scattering. First order corrections in $1/N$ to the leading result were shown to come from tree-level pion-quark scattering and quark-antiquark pair production diagrams. The latter contribution turned out to be logarithmically divergent but relatively small even for the values of a cutoff as large as 5 GeV.

In DOE-ER40200-291 Dicus, together with R. Vega (SLAC) and two Texas graduate students, D. Minic and U. van Kolck, elaborate on this last result. Following the same pattern of reasoning they also analyze the magnetic moment of the constituent quark using the same chiral Lagrangian and the analogue of the Drell-Hearn-Gerasimov sum rule for photon-quark scattering. The results seem to indicate that the chiral quark model with coefficients obtained by sum rules works well.

The value obtained for the axial vector coupling agrees within 20 percent with the experimental value. Perhaps the agreement could be improved by taking into account relativistic corrections. Concerning the anomalous magnetic moment, they show explicitly that the potentially dangerous $O(1/\sqrt{N})$ corrections are negligible. These results are evidence that the constituent quark model can be understood in the large N limit in terms of chiral symmetry (in the form of the chiral quark model) and reasonable assumptions on the high-energy behavior of amplitudes (embodied in sum rules).

Two papers by Dicus were reprinted in books in the past year. "Upper Bounds on the Value of Masses in Unified Gauge Theories" by Dicus and V. S. Mathur, originally published in Physical Review **D7**, 3111 (1973), was reprinted in *The Standard Model Higgs Boson* edited by M. B. Einhorn, CPSC Vol. 8. "Cosmological Upper Bounds on Heavy Neutrino Lifetimes" by Dicus, E. Kolb, and V. Teplitz, originally published in Physical Review Letters **39**, 168 (1977), was reprinted in *Cosmology and Particle Physics*, edited by D. Lindley, E. Kolb, and D. Schramm, American Association of Physics Teachers, 1991.

In DOE-ER40200-264, H. Baer (Florida State University), D. Dzialo Karatas, and G. F. Giudice (Theory Group, University of Texas) report on their use of a neural network to distinguish signal from background events in the single-lepton channel of top quark production at the Tevatron. They focus on the single-lepton channel of $t\bar{t}$ decay, in which one W decays leptonically and the other hadronically, as it offers the possibility of a direct determination of the top quark mass, since the presence of the single neutrino permits a kinematical reconstruction of the event.

They employ the feed-forward model of neural networks based on an input layer, a number of hidden layers, and an output layer. The training and testing event sets for top

quark production and the relevant W+multijet background are simulated by the Monte Carlo event generator PYTHIA at $p\bar{p}$ center of mass energy $\sqrt{s}$ =1.8 TeV subject to certain experimental acceptance requirements. They begin by training the neural network to distinguish between the top signal and the W plus multijets background; as inputs for the neural network they choose 10 kinematical variables to describe each event. The network performance is then tested by holding the weights fixed and confronting the nerual network with a fresh set of signal and background events. Correct signal (background) event classifications vary between 70% (80%) for a top quark mass of 100 GeV and 50% (96%) for a top quark of 140 GeV.

By making a cut on the network output, they maximize the ratio of signal to background in a final event sample, and compare these results with those corresponding to the best set of conventional kinematical cuts. The cut on neural network output is found to be more efficient than the set of conventional cuts as the ratio of signal/background that one obtains from the neural network is more favorable than the conventional cuts case by a factor of 1.9 for m_t =100 GeV, 3.5 for m_t =120 GeV, and the neural network is 7.7 more effective for m_t =140 GeV. There is a certain trade-off at play here in the favor of the neural network in that, as the cross section for the signal falls with increasing top mass, the neural network efficiency grows, whereas the ratio of signal/background for the severe cuts only suffers by the falling cross section for increasing top mass.

The authors also determine how well the neural network can succeed in identifying the top quark signal under realistic experimental conditions in which the top mass is not reliably known. For this purpose they train the neural network on signal events of one top mass and test it upon another. They find that the overall network performance is degraded by no more than 5% for the m_t = 100 GeV events, while overall network performance actually increases for the m_t = 140 GeV case. It is concluded in this report that by comparing such distributions with experimental data, one may not only confirm the existence of top quark events in the data sample, but may also extract a value for the top quark mass.

2.2.2 Relativistic Hamiltonian model for Higgs resonance

Higgs mechanism plays a crucial role in the unification electroweak theory. This mechanism also implies the existence of the Higgs particle. So far the Higgs particle has not been found. In the minimal standard model the bare mass of the Higgs is a free parameter. It is related to the coupling in the quartic interaction. It is well known that when the bare mass of the Higgs is large, the coupling is strong and here the gauge interaction of the Higgs and its

interaction with fermions are relatively unimportant. The theory for this case is referred to as the strong coupling theory. In DOE-259 and DOE-275, Professors Chiu, Sudarshan and Bhamathi are concerned with the prediction of the unified electroweak theory when the coupling is very strong. At the energy scale of 1 TeV which is significantly above the masses of W and Z, the interaction of Higgs with the gauge bosons is predominantly with the longitudinal components of the gauge bosons. The longitudinal components simulate an isotopic triplet of scalars. One may draw analogy between the interaction among this triplet and that among the pion triplet. For the pion case, there is the $I = S = 0$, sigma resonance. Analogously one may expect the Higgs resonance in the W^+W^- and ZZ channels. Various approaches have been used to investigate the occurrence of Higgs resonance. A partial list would include: the N/D method, the $1/N$ expansion in the $O(2N)$ model, and various "unitarization schemes". For the latter one finds that the Higgs resonance is present in the Padé approximation and is absent in the K-matrix approach.

In DOE-259 and DOE-275, Chiu, Sudarshan and Bhamathi constructed a relativistic Hamiltonian model for Higgs resonance. Resonance trajectories are studied as a function of the parameters of the model. The presence of Higgs resonance over a wide range of parameter values is found. Also it is possible to have Higgs resonance with moderate width, which can be "readily" detected at the supercollider energies. The numerical results of the present model may be used as a pheomenological guide in the search of Higgs in the sub–TeV and TeV region. An optimistic scenario is as follows: Through the interplay between model prediction and measurements, the data confirms one of the line shapes of the present model. This implies the discovery of Higgs resonance and at the same time it also predicts quantitatively the resonance pole position on the seecond sheet. This work, DOE-259, is published in Physical Review D.

2.2.3 Multiplicity Fluctuations at High Energies

The study of self-similarity in multiplicity fluctuations has been an active area of recent research. It began with the proposal of the intermittency phenomena by Bialas and Peschanski, i.e., a power-law behavior in the normalized factorial moments as functions of the rapidity bin width. Since then, this phenomenon has been observed in various collision processes, such as hadron-hadron, hadron-nucleus and e^+e^- processes. An extension of the intermittency phenomenon to multifractal analysis has also been considered by various authors.

DOE-274 is a talk which Dr. Chiu presented at the Ringberg Workshop on Intermittency and Multifractality. The work presented was done in collaboration with Professor

Rudolph Hwa of University of Oregon. A substantial portion presented was included in an earlier report of DOE-256. It is based on the JETSET Monte Carlo code of the Lund parton shower model. They confined their attention to the simplest process, the e^+e^- annihilation process, and study the multiplicity fluctuation as a function of s, the square of the cm energy, Y, the width of the rapidity window and N, the multiplicity in the window. The JETSET Monte Carlo program, which has successfully described the factorial moment data in e^+e^- annihilation process, provides a natural tool to carry out this study. One of their contributions is the suggestion of a "remedial cut-procedure" to accompany the multifractal analysis. This procedure enhances the scaling behavior signal. Based on the selected samples, they identify a certain universal property in the multifractal phenomena.

2.3 Quantum Mechanics and Quantum Field Theory

2.3.1 A Solvable Field Theory: The Cascade Model

To study scattering of resonances by particles Professor Sudarshan together with Professor Chiu and Professor G. Bhamathi constructed a Cascade model of interactions involving five fields, two of which (θ, ϕ) are light and the other (A, B, C) are heavy. This model is solvable explicitly. In particular in the three-particle sector $C\theta\phi$ have elastic and inelastic scattering and, in the latter domain, infinite degeneracy. They have found explicit solutions for both the scattering amplitudes and the generalized eigenvectors. These eigenvectors constitute the generalized Möller matrix which is unitary and diagonalizes the interacting Hamiltonian. In the three-particle sector, the eigenmodes of scattering are constructed and Newton's theorem verified. This paper DOE-279 is in course of publication in the Physical Review.

2.3.2 Analytic Continuation and Generalized Quantum States

In DOE-276, the method of analytic continuation of the spectrum and the state space of quantum systems discovered by Sudarshan, Chiu and Gorini has been applied to the study of the Lee model and the Cascade model by Professors Chiu and Sudarshan. They have obtained not only resonances poles but also complex branch cuts which can be identified as amplitudes for scattering of resonances of particles. These are shown to be analytic continuation of the amplitude for scattering of a bound state of particles. Various kinds of analytic continuations are described. A general theory of analytic continuation of inner product spaces is presented clarifying that the analytic relation is between dense sets. The choice of the dense sets defines the analytic continuation. The duals, considered as antilinear

functionals form the bra vector space $\tilde{\mathcal{G}}$ while the analytically continued space itself $\mathcal{G}$ is a distinct space. It is the dual pairs which are involved in the analytic continuation. This paper is submitted to the Physical Review for publication.

2.3.3 Theory of Neutral Kaons and Refined Bell-Steinberger Relation

In DOE-296, Professors Chiu and Sudarshan investigate the neutral kaon system using the general theory for the kaon decay complex. The exact solution is obtained. By deforming the unitarity cut to be along a contour Γ, an analytically continued theory, referred to as the "Γ theory" is obtained. A corresponding Γ^* theory may also be defined with the unitarity cut deformed along the complex conjugate contour Γ^*. Based on the theoretical work which involves both the Γ theory and the Γ^* theory, they derive an improved Bell-Steinberger relation. For the neutral kaon system, numerically, this generalized version can be reduced to the original Bell-Steinberger relation to a good approximation. It still remains to be a challenge to look for quantum processes in nature where the generalized version predicts a nonnegligible difference from the phenomenological Weisskopf–Wigner version.

2.3.4 Complex Quantum System

For many complex systems there are metastable excitations which decay and the decay is described by a semigroup of time evolutions rather then by the group of unitary Hamiltonian evolution appropriate in the Hilbert space. But a contractive semigroup requires that we study the evolution of a density matrix rather than a state vector. The analytic continuation of the quantum dynamics and the modification to the density matrix space has been studied by Profesor Sudarshan in DOE-270 which has been accepted for publication in the Physical Review.

The possibility using complex measures in stochastic processes started by Professor Sudarshan and Professor S. K. Srinivasan makes it possible to extend their scope to include superposition and diffraction. The Dirac-Feynman path integral formalism is a natural development. Hamiltonian evolutions and decay of correlations can be accommodated within complex measure stochastic processes. This work DOE-295 is being readied for publication.

Professor Sudarshan made an invited presentation to the Workshop on Uncertainty Relations in Moscow (organized jointly by the Lebedev Institute and the University of Maryland) on Canonical Invariance, Zero Point Energy and Uncertainty Relations with special reference to the group $Sp(2n, R)$ and its invariants. This work is to be published in the

10

Proceedings.

Professor Sudarshan attended the Santa Fe Workshop on Quantum Mechanics and made a contribution (DOE-266). This will be published in the Proceedings edited by Truman Black and Marlan Scully.

2.3.5 Skyrme Model

Sianiak S. Gousheh, working under the supervision of Prof. E. C. G. Sudarshan, has been studying the Skyrme model. He has used a modification of the adiabatic method of Goldstone and Wilczek to find the baryon number of Skyrmion in (3 + 1) in the nonadiabatic case. This paper, DOE-255, has been published in Physical Review D. He also has used the above method in (1 + 1) for a more general case. In this method, the energy spectrum of baryons, coupled to a background chiral field, are monitored as the chiral field is adiabatically deformed to a topological charge one configuration (i.e., a Skyrmion). It is found that in general there are many bound states and only for a Skyrmion with sufficiently sharp features (nonadiabatic case) one energy level crosses zero from above. Furthermore, it is shown explicitly that the Dirac sea is missing one level regardless of the shape of the Skyrmion in finite distances and the continuum states alone do not form a complete set. Thus this confirms the Goldstone-Wilczek's adiabatic result and shows that it also holds in the nonadiabatic case except that it has to be supplemented by possible level crossing. Thus in the (1 + 1) model studied it is shown that the vacuum in the presence of only slowly varying Skyrmions carries baryon number.

2.3.6 Finite Temperature QED

Samir Varma, working under the supervision of Professor Sudarshan, studied the temperature-dependence of the Compton scattering amplitude and its radiative corrections generalizing earlier (unpublished) work of Sudarshan, Glashow and Yildiz and the published work (Phys. Rev. D 29, 2694 (1982)) of Dicus, Kolb, Gleeson, Sudarshan, Teplitz, and Turner on nucleosynthesis. Other previous studies had primarily focused on the calculation of the renormalization constants and there had been very few studies of the corrections to fundamental processses. He chose to calculate the corrections to the Compton Scattering cross section because it is used to calculate stellar opacity, relic radiation and many other important processes. This involved carrying out detailed analytical and numerical work in computing the expected cross section which included calculating the finite temperature mass and wave-

function renormalization constants for the electron. This paper, DOE-290, is submitted to the Physical Review for publication.

2.3.7 String Field Theory

Akinobu Ukegawa, working under the supervision of Professor Sudarshan, completed his doctoral work on string field theory and submitted a thesis titled "Off-Shell Amplitudes in Covariantized Light-Cone Open and Closed String Field Theories" (Spring 1991). Several papers (DOE-237, 238 and 239) based on this thesis are submitted for publication.

2.3.8 Options for a Laser Accelerator

Steve Maxson under Professor Sudarshan's supervision has extended extended some earlier work of Prof. Sudarshan on a "first principle" description of thin paraxial lenses to include optical quadrupole lenses for possible use in a laser accelerator. Maxson showed that such lenses would degrade the coherence of the laser acceleration field (unacceptably).

2.3.9 Geometric Phase and the Projective Hilbert Space

Professor Sudarshan in collaboration with Professor J. Anandan and Dr. T. R. Govindarajan (who was a visitor to the Center for Particle Theory) defined a new unitary operator in the Hilbert space of a quantum system which parallel transports the state of the system along an arbitrary curve in the projective Hilbert space. This geometric operator is defined even for an open arc; when the curve is closed, the geometric phase discovered by Pancharatram, by Berry and by Aharanov and Anandan is recovered. Thus this is the generalization of the Berry phase. This paper, DOE-294, is published in Physics Letters.

3 Titles of DOE Reports Since DOE-ER-40200-262

DOE-ER40200-263	Isolating Purely Leptonic Signals for Strong W Scattering Using Anti-Tagging, Jet-Tagging and Lepton Isolation, by Duane A. Dicus, J. F. Gunion, L. H. Orr, and R. Vega
DOE-ER40200-264	Snagging the Top Quark with a Neural Net, by Howard Baer, Debra Dzialo Karatas, and Gian F. Giudice
DOE-ER40200-265	Quantum Mechanics, Metastable States and Contrative Semigroups, by E. C. G. Sudarshan
DOE-ER40200-266	Measurement Theory, by E. C. G. Sudarshan
DOE-ER40200-267	$I = 1, J = 1$ Resonances in the Padé Unitarized WW Scattering Amplitude, by Duane A. Dicus and Wayne W. Repko
DOE-ER40200-268	Proof of Pseudo-Gravity as QCD Approximation for Hadron IR Region and JM^2 Regge Trajectories, by Y. Ne'eman and Dj. Sijacki
DOE-ER40200-269	The Geometric Phase in Quantum Physics, by A. Bohm
DOE-ER40200-270	The Structure of Quantum Dynamical Semigroups, by E. C. G. Sudarshan
DOE-ER40200-271	How can we find the exotics? by G. Bhamathi
DOE-ER40200-272	Squeezing of Light Within the Framework of Population Theoretic Approach, by S. K. Srinivasan
DOE-ER40200-273	Superconnections and Internal Supersymmetry Dynamics, by Yuval Ne'eman and Shlomo Sternberg
DOE-ER40200-274	Intermittency and Multifractality in Monte Carlo e^+e^- Annihilation, by Charles B. Chiu
DOE-ER40200-275	Relativistic Hamiltonian Model for Higgs Resonance, by Charles B. Chiu, E. C. G. Sudarshan, and G. Bhamathi
DOE-ER40200-276	Analytic Continuation of Quantum System and Their Temporal Evolution, by E. C. G. Sudarshan, and Charles B. Chiu
DOE-ER40200-277	Symplectic Structure of the Aharonov-Anandan Geometric Phase, by Luis. J. Boya, José F. Carinena and José M. Gracia-Bondía
DOE-ER40200-278	$SU(2/1)$ as Chiral Supersymmetry, by Y. Ne'eman
DOE-ER40200-279	The Cascade Model: A Solvable Field Theory, by E. C. G. Sudarshan, Charles B. Chiu and G. Bhamathi
DOE-ER40200-280	A Parallelism between Quantum Gravity and the IR Limit in QCD, by Y. Ne'eman
DOE-ER40200-281	$SU(2/1)$, Superconnections and Geometric Higgs Fields, by Y. Ne'eman, C-Y. Lee and Dj. Sijacki

DOE-ER40200-282	The Metaplectic Action and Phases in the Wigner-Moyal and Bargmann Representations, by José Gracia-Bondía
DOE-ER40200-283	Representations of Infinite Dimensional Groups in Quantum Field Theory. I. The Metaplectic Representation and Boson Fields, by José Gracia-Bondía and Joseph C. Várilly
DOE-ER40200-284	S-matrix from the Metaplectic Representation, by Joseph C. Várilly and José Gracia-Bondía
DOE-ER40200-285	Representations of Infinite Dimensional Groups in Quantum Field Theory. II. The Pin Representation and Fermion Fields, by Joseph C. Várilly and José Gracia-Bondía
DOE-ER40200-286	Spin Representation and Feynman Rules, by Joseph C. Várilly and José Gracia-Bondía
DOE-ER40200-287	Toward a Conformal Field Theory for the Quantum Hall Effect, by Greg Nagao
DOE-ER40200-288	Connections Between CFT and the Quantum Hall Effect, by Greg Nagao
DOE-ER40200-289	Wigner Analysis and Casimir Operators of $SA(4, R)$, by Juergen Lemke, Yuval Ne'eman and Jose Pecina-Cruz
DOE-ER40200-290	Finite Temperature Radiative Corrections to Compton Scattering, by S. Varma
DOE-ER40200-291	The Axial Vector Coupling and Magnetic Moment of the Quark, by Duane A. Dicus, D. Minic, U. van Kolck, and R. Vega
DOE-ER40200-292	The Pseudo-Gravity Approximation in QCD for Particles and Nuclei, by Y. Ne'eman
DOE-ER40200-293	The Berry Connection and Born-Oppenheimer Method, by A. Bohm, B. Kendrick, Mark E. Loewe and L. J. Boya
DOE-ER40200-294	A Group Theoretic Treatment of the Geometric Phase, by E. C. G. Sudarshan, J. Anandan, and T. R. Govindarajan
DOE-ER40200-295	Complex Measures and Amplitudes, Generalized Stochastic Process and Their Applications to Quantum Mechanics, by E. C. G. Sudarshan
DOE-ER40200-296	Theory of the Neutral Kaon System, by Charles B. Chiu and E. C. G. Sudarshan

Progress Report

of

Task B

Experimental

1 Introduction

Calendar year 1992 is the third full year of DOE funding of experimental high energy physics research at the University of Texas at Austin. Several milestones were (or will be — this report is being written in June, 1992) passed during this period. Among them are the publication of final results from Expt. 791 at the AGS facility at the Brookhaven National Laboratory; this experiment has proved to be the most sensitive search for rare kaon decays ever conducted. An upgrade of this experiment, Expt. 871, is being constructed. Also, a side experiment, E888, using the E791 spectrometer, was conducted to search for an H dibaryon during May and June at the AGS. Finally, detector simulation and design studies are advancing for the GEM detector for the SSC.

2 Status of BNL Expt. 791

Experiment 791 was performed in the B5 neutral beam at the Alternating Gradient Synchrotron at the Brookhaven National Laboratory. The spectrometer combined precise tracking with good particle identification capability.[1, 2] High rate capability was achieved by fully-custom high speed front-end electronics,[3, 4] a massively parallel readout architecture,[5] and a multi-level trigger system utilizing SLAC 3081/E emulators.

E791 ran in three consecutive years at the AGS (1988, 1989, and 1990). Results from the 1988 data on the decays $K_L \rightarrow \mu e$, $K_L \rightarrow ee$, and $K_L \rightarrow \mu\mu$ have been published[2, 6]. A measurement of the $K_L \rightarrow \mu\mu$ branching ratio from the 1989 data has been published.[7] The final analysis of the 1990 data has been completed and a Physical Review Letter is in preparation. These results have been reported in conferences.[8] Final publications on the $K_L \rightarrow \mu\mu$ branching ratio and a limit on the $K_L \rightarrow ee$ decay will also be completed in the near future.

E791 has been the most successful search for $K_L \rightarrow \mu e$ to date. The final limit, 3.3×10^{-11} (90% confidence level), is the lowest sensitivity ever achieved in any kaon experiment. The final E791 results are summarized in Table 1, along with the other recent $K_L \rightarrow \mu e$ searches. Figure 1 shows a scatter plot of missing transverse momentum versus reconstructed invariant mass for $K_L \rightarrow \mu e$ candidates in E791. No events appear in the signal box.

	BNL780	KEK137	BNL791
$K_L \rightarrow \mu e$ limit	1.9×10^{-9}	9.4×10^{-11}	3.3×10^{-11}
$K_L \rightarrow ee$ limit	1.2×10^{-9}	1.6×10^{-10}	4.1×10^{-11}
$K_L \rightarrow \mu\mu$ sample	~ 8 events	178 ± 13 events	717 ± 27 events

Table 1: Results from recent $K_L \rightarrow \mu e$ searches.
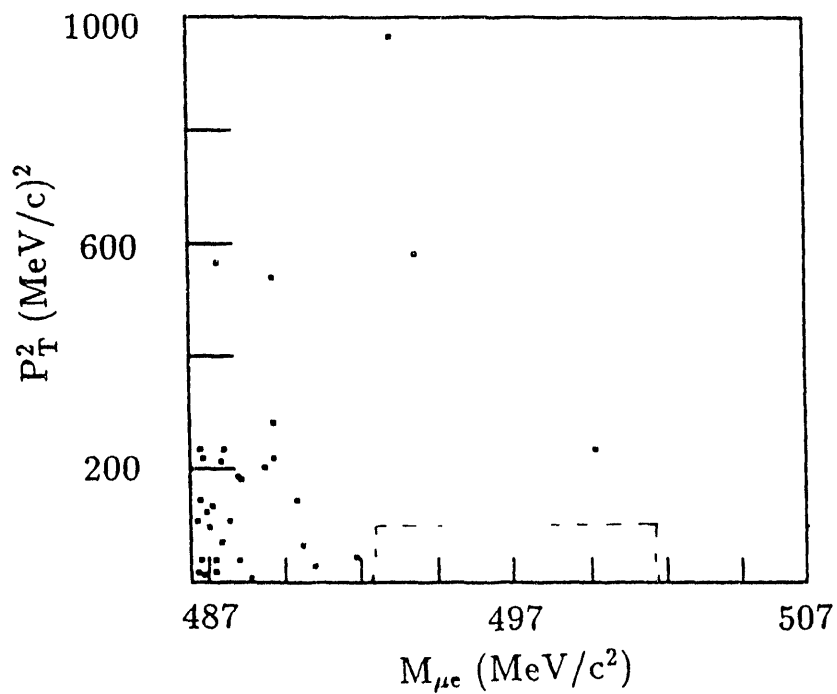
Figure 1: Scatter plots of the square of the missing transverse momentum, p_T^2, versus invariant mass, for $K_L \rightarrow \mu e$.

3 BNL Expt. 871

Expt. 871 received final approval in August, 1991. Some operating parameters of E871 are summarized in Table 2. The ultimate sensitivity of E871 will be at the 10^{-12} level.

K_L in beam/spill	2×10^8
Fraction of K_L's decaying with $1.7 < p_K < 20$ GeV/c and 11.5 m $< z_{DK} < 26$ m	0.11
K_L decays in normalization region/spill	2.2×10^7
Spills/hour	1200
Beam hours/week	100
K_L's in 38 weeks of running	1×10^{14}
$K_L \rightarrow \mu e$ acceptance	0.0242
Particle id efficiency (μe)	0.9
Trigger efficiency	0.85
Pattern recognition eff. (analysis cuts)	0.7
Running efficiency	0.92
Net efficiency (incl. acceptance)	0.012
Single event sensitivity	8.3×10^{-13}
90% confidence level sensitivity	2×10^{-12}

Table 2: Some operating parameters expected in E871.

A novel feature of E871 is the use of a neutral beam stop, or plug, inside the spectrometer. It was necessary to perform extensive beam tests to prove that the plug design was successful in suppressing detector rates to acceptable levels. Also, results of the beam test have helped to advance the design of the detector. The UT Austin group took a leading role in mounting these tests and the subsequent data analysis. Consequently, below some details of this work are provided.

3.1 Overview of the Test Run

The run began at the beginning of April. The first three weeks were spent on routine detector commissioning and a series of tests to investigate some of the sources of detector rates in E791, including beam scraping on chambers, low energy neutrons and photons from the upstream shielding, and electronic noise. Subsequently, plug studies went on for about three weeks, followed by a four week hiatus in E871 running (during which another experiment had control of the B-line). A significant modification was made to the plug, including the addition of heavimet, during this month off. Finally, the last two weeks of June were spent on further plug studies.

The plug consisted of a core of non-magnetic heavimet, a tungsten-copper alloy of density 18 g/cm^3, backed up by copper, and surrounded with 0.5% borated polyethylene, a thin layer of a highly (30%) borated material (trade name Boroflex), and finally by a layer of lead. The dense core attenuates hadronic showers quickly; the polyethylene moderates neutrons escaping the metallic core. Once thermalized, neutrons are captured on the boron. The lead prevents the 480 keV photons, produced when the thermal neutrons are captured, from escaping. The nominal depth (in the beam direction) of heavimet was 112 cm, followed by 40 cm of additional copper. The requirement that the plug be narrow in the horizontal x direction, to preserve the E871 acceptance, is what makes the plug design difficult. The nominal width of materials was 30 cm of heavimet, 5 cm of polyethylene on each side, 0.32 cm on Boroflex of each side, and 0.64 cm of lead on each side — making a total width of 42 cm. The beam entered a tunnel before interacting in the plug. The depth of the tunnel was 80 cm; the upstream 50 cm consisted of polyethylene layered with lead and the final 30 cm of the tunnel consisted of heavimet. During the course of our tests, the dimensions of the plug, thickness of the shielding materials, composition and size of the tunnel, etc., were varied to gain an understanding of detector rates as a function of the details of plug construction. Ultimately, the heavimet core was widened to 35.5 cm. Also, some copper plates were tested as shielding on the outside.

The data from which detector rates were measured were taken by triggering the E791 detector with a pulse generator, providing events which were effectively random with respect to any beam associated process. Two or three tapes, each containing about 230,000 such pulser events, were written for a large number of distinct configurations of the plug or local

shielding. Most of these amounted to incremental modifications with the goal of isolating the dependance of specific detector rates on particular plug features. In all, data were taken for about 80 distinct shielding configurations. Figure 2 shows the layout of the E791 spectrometer. The plug was located in the 96D40 spectrometer magnet. Data were usually taken with the magnetic field both on (i.e., at a field of about 1.2 Tesla, within 10-15% of the full field planned for E871) and off — and in some cases with the polarity reversed.

The normalization of detector rates to the beam flux onto the plug was done in several different ways. The most reliable is to count two-track vertices (V's) in the decay volume, using the two upstream E791 drift chambers. This method normalizes to kaon flux, which should be fixed with respect to neutron flux. A limitation of this method is statistical since most pulser tapes contain only a few hundred V's. Other methods were not statistically limited, but suffered from systematic variations. For example, two scintillation counter telescopes act as 90° monitors for the proton target. While the two telescopes track each other closely, comparisons with other monitors show that they are sensitive to changes in targeting. In general, the cross normalization of different runs is the biggest difficultly we have encountered in analyzing and understanding plug data.

In addition to E791 detector rates, measurements were made with a set of special detectors to investigate the flux and energy distributions of low energy neutrons and photons from the plug. These consisted of:

- Liquid scintillators. Because of the difference in shape of pulses caused by neutrons and photons, these detectors can separate neutrons and photons in the energy range of about 0.1 MeV to 10 MeV for photons and 0.6 MeV to 10 MeV for neutrons. The pulse height spectra can also be unfolded to provide some information on the energy spectra. The liquid scintillators were partly surrounded by plastic scintillators, which provided the ability to veto charged particles.

- Bonner spheres. These are spherical polyethylene neutron moderators which enclose a LiI(Eu) scintillator. By counting thermal neutron captures on the lithium for a series of different sized spheres, it is possible to obtain information on the neutron energy spectrum from thermal energy up to about 25 MeV.

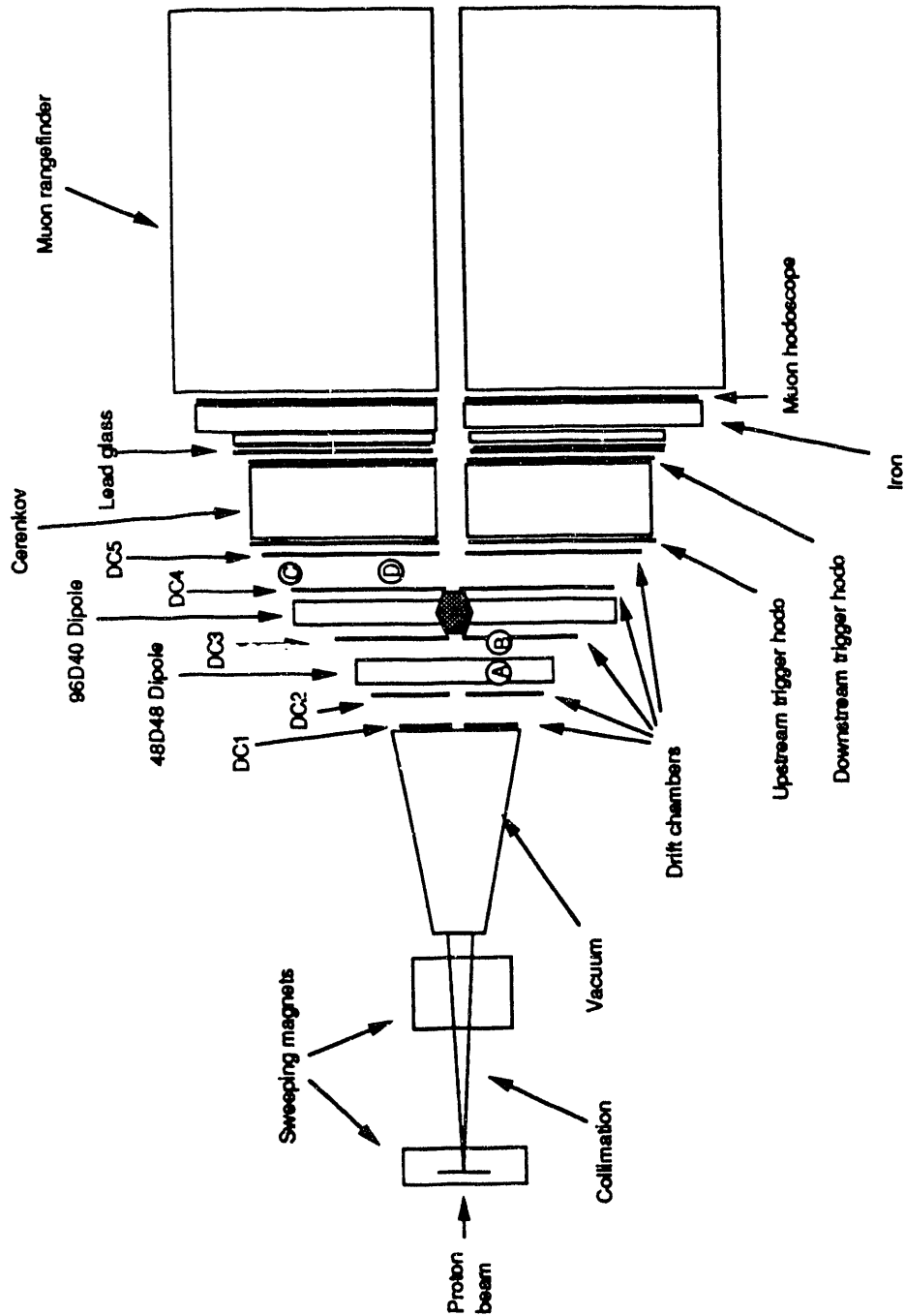- ^{3}He counters. These are gas counters which count very low energy neutrons through

20

Figure 2: Plan view of the E791 spectrometer used for plug tests. The upstream dipole magnet was not used. The downstream 96D40 dipole, where the plug was located, was run at a field of about 1.2 Tesla — about 10-15% below the full E871 field. The locations at which the neutron and photon detectors were located are indicated by the circles enclosing the letters A, B, C, and D.

the interaction $^3He(n,p)^3H$, which has a 4000 barn cross section at thermal energy and decreases inversely with the neutron's velocity. In our case, neutrons were observed from thermal energy up to about 20 eV.

- Solid state germanium detector. This detector provides high resolution measurements of photon energy spectra.

Data were taken with these detectors for most of the plug configurations tested. However, the Bonner sphere measurements, which are time consuming, were made only after major plug modifications.

The neutron and gamma detectors were read out with a stand-alone data acquisition system, so that V's cannot be used to normalize these measurements. However, a number of scalers generated from signals from the E791 detector, as well as the 90° telescopes and other beam associated quantities, were recorded and can be used for normalization and cross checks.

3.2 Neutron and Photon Measurements

The purpose behind operating the neutron and photon detectors was two-fold: (1) understanding the physics of the plug (for example, comparisons with the HETC-MORSE Monte Carlo) requires direct knowledge of the low energy particles escaping the plug and (2) understanding the sources of detector rates is very difficult without knowledge of the fluxes of low energy particles.

Prior to the plug test, we were very concerned about neutrons as a major source of detector rates. We now believe that the interaction of neutrons in detectors is not a problem indicating the basic plug design is highly successful. A strong statement regarding photons is more difficult. Photons in the energy range covered by the liquid scintillators, from about 100 keV up to 10 MeV, do not account for a significant fraction of the rate in drift chambers or scintillators.

Figure 3 shows a scatter plot of ADC pulse heights (from an early short gate and a long late gate) from one of the liquid scintillators. The separation between the neutron and photon bands can clearly be seen. The calibration of these detectors was established with radioactive sources (^{22}Na for photons and ^{252}Cf for neutrons). Since charged particles also register in
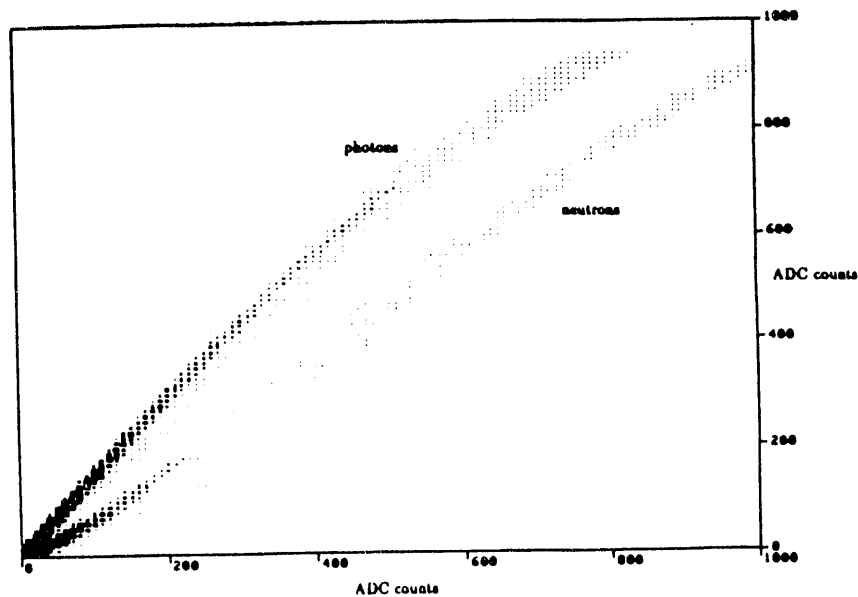
Figure 3: Pulse shape discrimination of neutrons and photons using the liquid scintillators. The vertical axis is the pulse height from a "prompt" gate, which is 50 ns wide and is timed to coincide with the peak of the phototube pulse. The horizontal axis is the pulse height from a "delayed" gate, which is 100 ns wide and is timed to cover the tail of the phototube pulse.

the liquid scintillators, these counters were operated between two plastic scintillators which could veto charged particles. In addition to vetoing, however, the coincidence of the liquid scintillator with the plastic scintillators could also count the charged particle flux. Therefore, with these detectors we ultimately have measurements of the neutron, photon, and charged particle fluxes — at least over the energy ranges covered by these detectors.

Figure 4 shows the results of a Bonner sphere measurement of neutrons at a location upstream of the plug where one of the E791 drift chambers — DC3 — is normally located; this is the position B indicated in Figure 2. Figure 4 shows the number of neutrons versus energy from thermal energy up to 25 MeV. The results are shown for three different configurations: no plug, a plug consisting of only the metallic core (heavimet and copper), and a fully shielded plug. We can compare the Bonner sphere results to ^{3}He counters at the low energy end of the spectrum and to the liquid scintillator pulse shape discrimination measurements in the range of a 0.6 to 10 MeV. We find in both cases that the agreement is typically good to 25% for the full set of Bonner sphere measurements. Having a full neutron spectrum, it is then possible to estimate detector rates from neutron interactions by integrating the
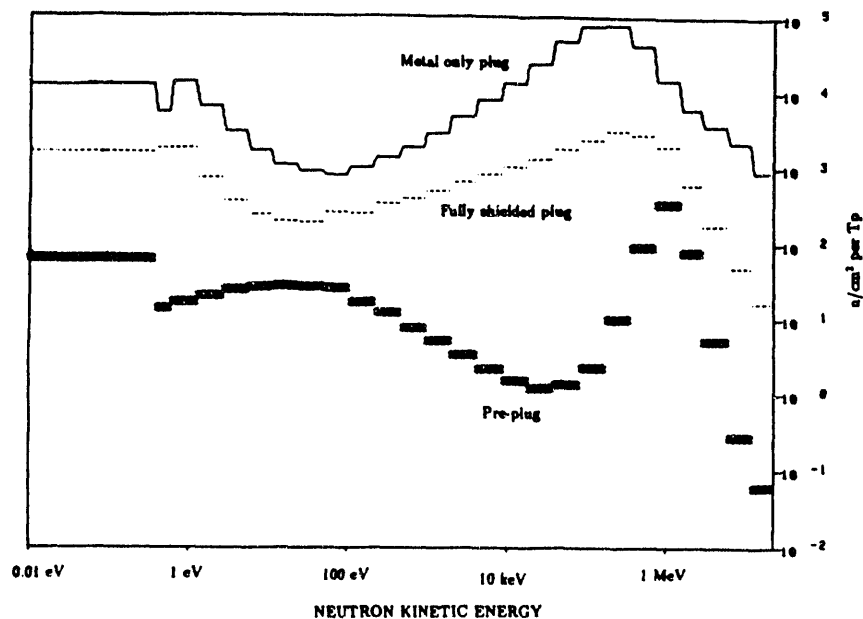
23

Figure 4: Neutron flux versus energy as measured with Bonner spheres for three plug configurations. The vertical scale gives neutron flux in units of neutrons/cm^2 per Tp of incident protons on target. The horizontal scale is neutron kinetic energy. Both the horizontal and vertical scales are logarithmic.

measured spectrum against known neutron interaction cross sections.

We have used this information to predict the rates in E791 detectors. Comparing these predictions to the measured rates indicates the level at which the sources of detector rates are.understood. Such a comparison is made in Table 3 between predicted and measured drift chamber rates. We will not describe the details of the underlying calculations here. Details are contained in a series of internal E791/E871 memos.

For the purpose of this comparison, the relevant number from the drift chambers is the rate of single particle interactions, not the rate at which wires are hit. This is because a single particle may cause one, two or more wires to be hit. To account for this we have defined "clusters" in the drift chambers; that is, we have counted groupings of hit wires as a single interaction. Since the neutron detectors could not be normalized to V's, we have used one of the 90° telescopes, denoted B5T1.

The measurements on which the estimates in Table 3 are based were made in the actual position of DC3-right, while that chamber was removed (position B). For DC4 and DC5, data were taken with the neutron and photon detectors about half way between these chambers in z; see Figure 2 for locations C and D. Practical considerations drove the positions of these

PRE-PLUG					
Chamber/Position	Neutrons	Photons	Charged	Total	Measured
DC 3 / B	0.40	10.1	345	355	627
DC 4 / C	0.16	5.06	166	171	938
DC 4 / D	—	12.9	770	—	938
DC 5 / C	0.19	5.92	194	220	904
DC 5 / D	—	15.1	898	—	904
METAL ONLY PLUG					
Chamber	Neutrons	Photons	Charged	Total	Measured
DC 3 / B	260	146	746	1152	3942
DC 4 / C	97.5	89.9	410	597	3011
DC 4 / D	—	78.6	400	—	3011
DC 5 / C	118	105	478	701	1288
DC 5 / D	—	91.9	467	—	1288
SHIELDED PLUG					
Chamber	Neutrons	Photons	Charged	Total	Measured
DC 3 / B	19	45.2	367	431	1196
DC 4 / C	8.6	23.3	245	277	1254
DC 4 / D	—	24.0	289	—	1254
DC 5 / C	10.3	27.2	285	323	522
DC 5 / D	—	28.1	337	—	522

Table 3: Comparison of the predicted and measured number of particle interactions in drift chambers, per B5T1 count. Neutron estimates are based on Bonner sphere results; photons and charged particles are based on liquid and plastic scintillators. The letter (B, C, or D) in the first column refers to the positions of neutron/photon detectors shown in Figure 2. Estimates of DC3 rates are based on position B, which is at the DC3 position. Estimates for rates in DC4 and DC5 are based on positions C and D. We have taken the neutron, photon, and charged particle fluxes to be uniformly distributed across the chambers. No Bonner sphere measurements were made at position D. For these measurements, the magnet was off.

measurements. Since we do not know the position dependence of the particle fluxes, we have assumed uniform illumination of chambers and, for DC4 and DC5, we have used the flux measured at the single z position between the two. This probably leads to a low value for DC4 and a high value for DC5 for the configurations with a plug.

As can be seen from the table, pre-plug rates can roughly be accounted for by charged particles. However, the sum of neutrons, photons, and charged particles do not account for more than about 30% of the measured interaction rates in DC3 and DC4 for the metal only or shielded plugs. The discrepancy may be due to either photons or charged particles of energy below the sensitivity of the detectors. Nonetheless, if neutron interactions in the drift chambers are dominated by the reaction $n + p \rightarrow n + p$ in the gas as we believe, then neutron interactions cannot account for a significant fraction of the observed rates.

3.3   Drift Chamber Rates

The biggest question associated with the plug is the feasibility of operating drift chambers in close proximity to the plug itself. In this section we will first present measurements of drift chamber rates made in three different plug configurations. For assessing performance, the fully shielded plug, which was the best case plug in the 1991 test run, should be taken as the worst case for the future; further studies and plug improvements may lower rates compared to the 1991 test. After discussing the measured rates, we will describe the features of the proposed E871 tracking detectors that we believe will allow us to operate in proximity to the plug.

The E791 spectrometer has 20 drift chamber planes, if x and y are counted separately for chambers on both the left and right sides of the beam. However, these chambers are located at only five different positions in z. The locations of chambers with respect to the plug can be seen in Figure 2. Figure 5 shows chamber rates in units of hits/V for three different configurations: no plug, metal only plug, and the fully shielded plug. It should be kept in mind that the more downstream chambers have larger area and more wires, so total rates are not an indication of single wire occupancy; they are presented for the purpose of comparing different plug configurations. These rates were measured with the 96D40 magnet on; some rates depended on the condition of the magnetic field. While the figure shows that the rates with the unshielded "metal only" plug skyrocketed, the effect of the shielding

was also dramatic. With the fully shielded plug, drift chamber rates were roughly double pre-plug rates in DC3 and DC4, which were very close to the plug. Rates in other chambers are higher with the shielded plug than no plug, but generally at the 30% level.

Figure 6 shows the illuminations of hits for DC3X-left and DC5X-left for the pre-plug and shielded plug cases. These illuminations illustrate a general feature of detector rates — that they are more uniform across detectors — in the presence of the plug.

In order to address the issue of the effect of these rates, Figure 7 shows the rates for the shielded plug in terms of the single wire rates. The rates are presented in units of KHz, scaled to a proton intensity of 15 Tp/spill, the intensity necessary to reach our proposed E871 sensitivity in 4000 hours of running. The rates are high and it would not be prudent to operate the E791 drift chambers under these conditions. Nonetheless, we believe that a combination of smaller cell sizes, additional planes of wires, and faster gas, will make it possible to operate new drift chambers near the plug.

Our conclusion that rates in chambers such as we are now proposing are acceptable is based on an estimate of the occupancy. We believe this is the simplest way to quantify the effects of rates upon the pattern recognition power of the spectrometer; that is, how often a correct hit will be corrupted because of a false hit. As can be seen from Figure 7, a typical wire rate in the E791 chambers was about 600 KHz when scaled to 15 Tp/spill. The corresponding occupancy is 4.5%. This is based on a TDC livetime of 150 ns and the fact that 1/2 of the false hits will occur later than the true hit (i.e., doing no harm). Reducing the cell size from 1 cm to 0.5 cm will reduce the rate on each wire by a factor of two and the occupancy by a factor of four. Replacing our current drift chamber gas (Ar-C_2H_6) with a faster gas (e.g., Ar-CF_4), will further reduce the occupancy by the ratio of the drift speeds - about a factor of 1.9, since the speeds are approximately 50 μm/ns versus 95 μm/ns. Therefore, the typical occupancy in an E871 chamber would be 0.6%. The highest wire rates occurred in chamber DC 3-right, on the inner x measuring wires. The rates were about 1.3 MHz when scaled to 15 Tp/spill. This implies a single wire occupancy of 1.3% for the worst wire in E871. Addition of an extra plane of x measuring wires will provide further protection against accidental hits. For the sake of comparison, the hottest wire occupancy for E791 operating at 4.5 Tp/spill (the intensity at which physics data were taken during the 1990 run) was 1.8%.

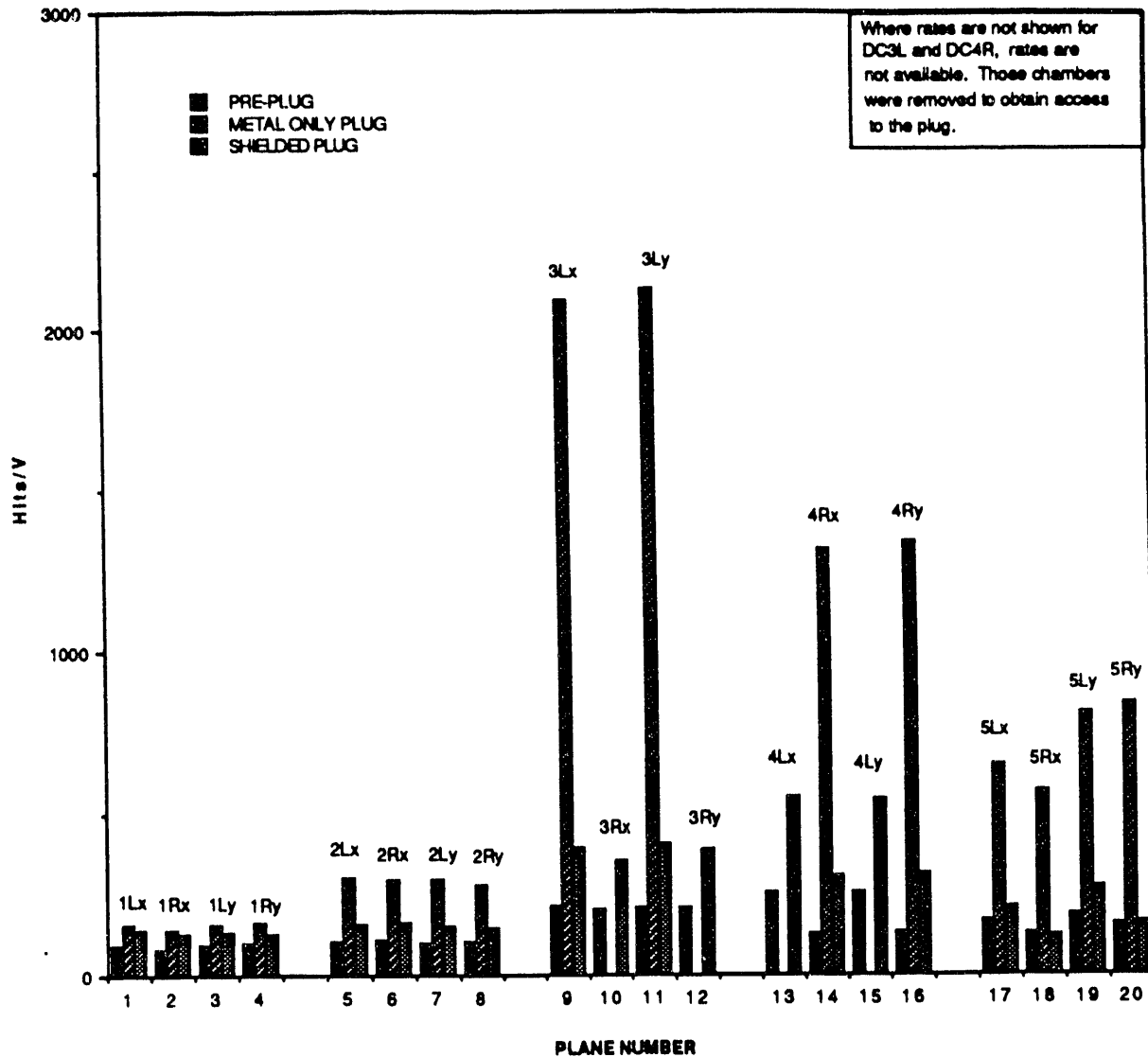Tests with a prototype straw chamber near the plug indicated that rates with Ar-CF_4

Figure 5: Hits/V for all E791 drift chamber planes for three configurations of the plug. The columns are labeled for each drift chamber. For example, 3Lx refers to the DC 3 left-side x measuring plane. To convert from hits/V to hit/sec, multiply by 23,000 V/Tp-sec. For example, 100 hits/V corresponds to a rate of 2.3 MHz at 1 Tp/spill. (1 Tp = 10^{12} protons on target).
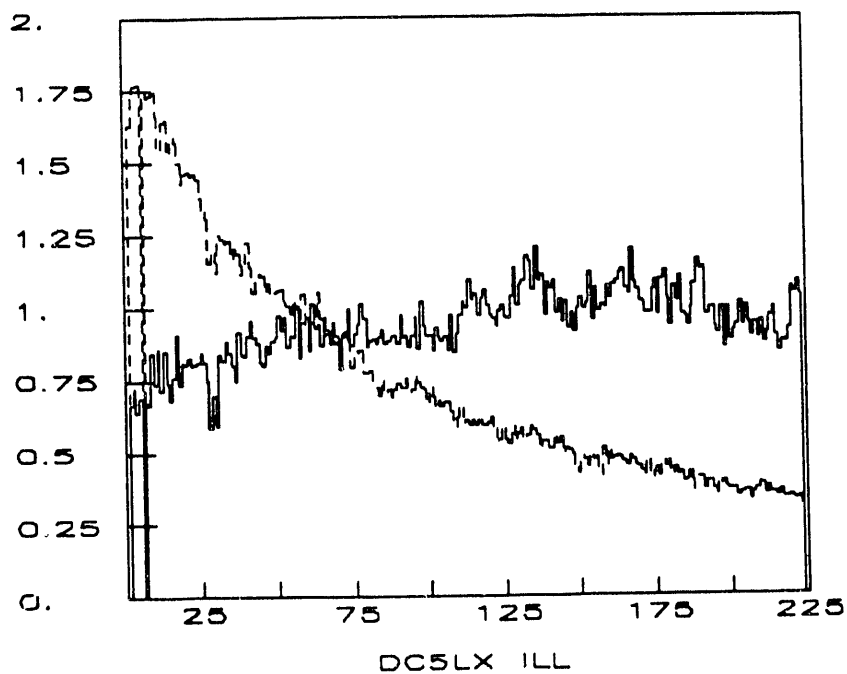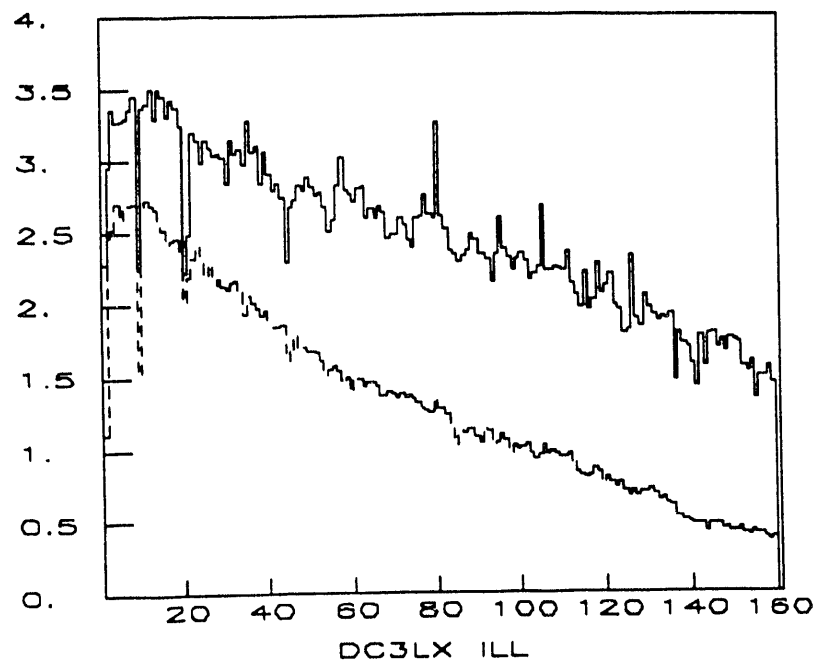
Figure 6: Drift chamber illuminations for DC3X-left (top) and DC5X-left (bottom) for the pre-plug (dashed line) and fully shielded plug (solid line) configurations. The vertical scale is Hits/V per wire. Each horizontal bin corresponds to a drift chamber wire.

Average Drift Chamber Single Wire Rates for the pre-plug and fully shielded plug configurations.
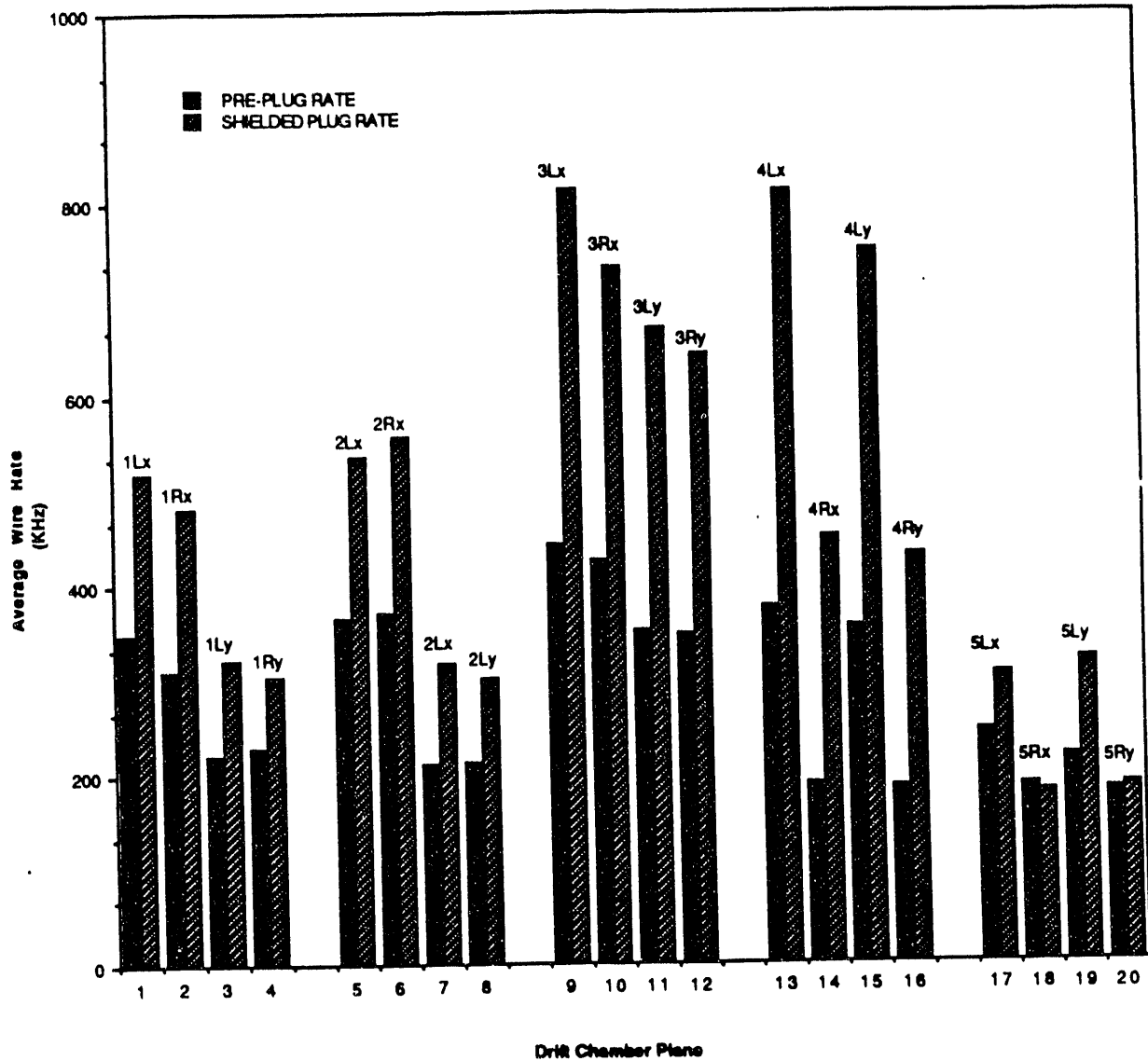
Figure 7: Average wire rates for each E791 drift chamber in KHz when scaled to a proton intensity of 15 Tp/spill. The columns are labeled for each drift chamber. For example, 3Lx refers to the DC 3 left-side x measuring plane.

are similar to those with Ar-C_2H_6. Therefore, we no are not hopeful that a gas without hydrogen will lead to lower rates. This is consistent with the conclusion, discussed earlier, that direct interaction of neutrons in chambers is not a significant source of rate.

3.4 Trigger Counter and Particle ID Rates

There are two scintillation counter trigger hodoscopes in the E791 setup. Rates in these counters were measured in the same fashion as drift chamber rates and are shown in Figure 8. The location of these counters can be seen in Figure 2. Rates are again given in terms of hits/V. Rates for counters in Figure 8 are defined so that they are directly comparable to the drift chambers rates in Figure 5. Consequently, to convert these numbers to hits/second, the same factor as for drift chambers (23,000 V/Tp-sec) should be used. The figure also includes rates for the Čerenkov counter, lead glass array, and the muon hodoscope counters. The Čerenkov rates are given for one quadrant of the full counter, since tests using the other tubes were being conducted simultaneously with these measurements.

The results shown in Figure 8 apply to counter banks with differing numbers of individual photomultipliers. Table 4 gives the average rates for single channels of each of these detectors for the fully shielded plug. The rates are quoted in KHz and have been scaled to a proton beam intensity of 15 Tp/spill.

·The upstream trigger hodoscope in the E791 setup is more than a meter closer to the plug than the corresponding E871 hodoscope will be. Note from Table 4 that the rate in the upstream trigger hodoscope for the shielded plug is about 2.5 times higher than the downstream trigger hodoscope, which covers the same area. The distance between these hodoscopes is about 3 meters. It is likely, therefore, that a hodoscope at the E871 location would see a significantly lower rate than the value listed in the table.

The Čerenkov hit rates shown in both Figure 8 and Table 4 do not reflect the reduction that can be made by locally shielding the photomultiplier tubes. Tests using borated polyethylene and lead indicated that about 2/3 of the plug induced rate can be eliminated. Also, ADC pulse height spectra show that the plug induced Čerenkov hits essentially all occur at the single photoelectron level. If the new E871 counter delivers the six or more photoelectrons on average that we expect, then thresholds can be set at the two photoelectron level without loss of efficiency.
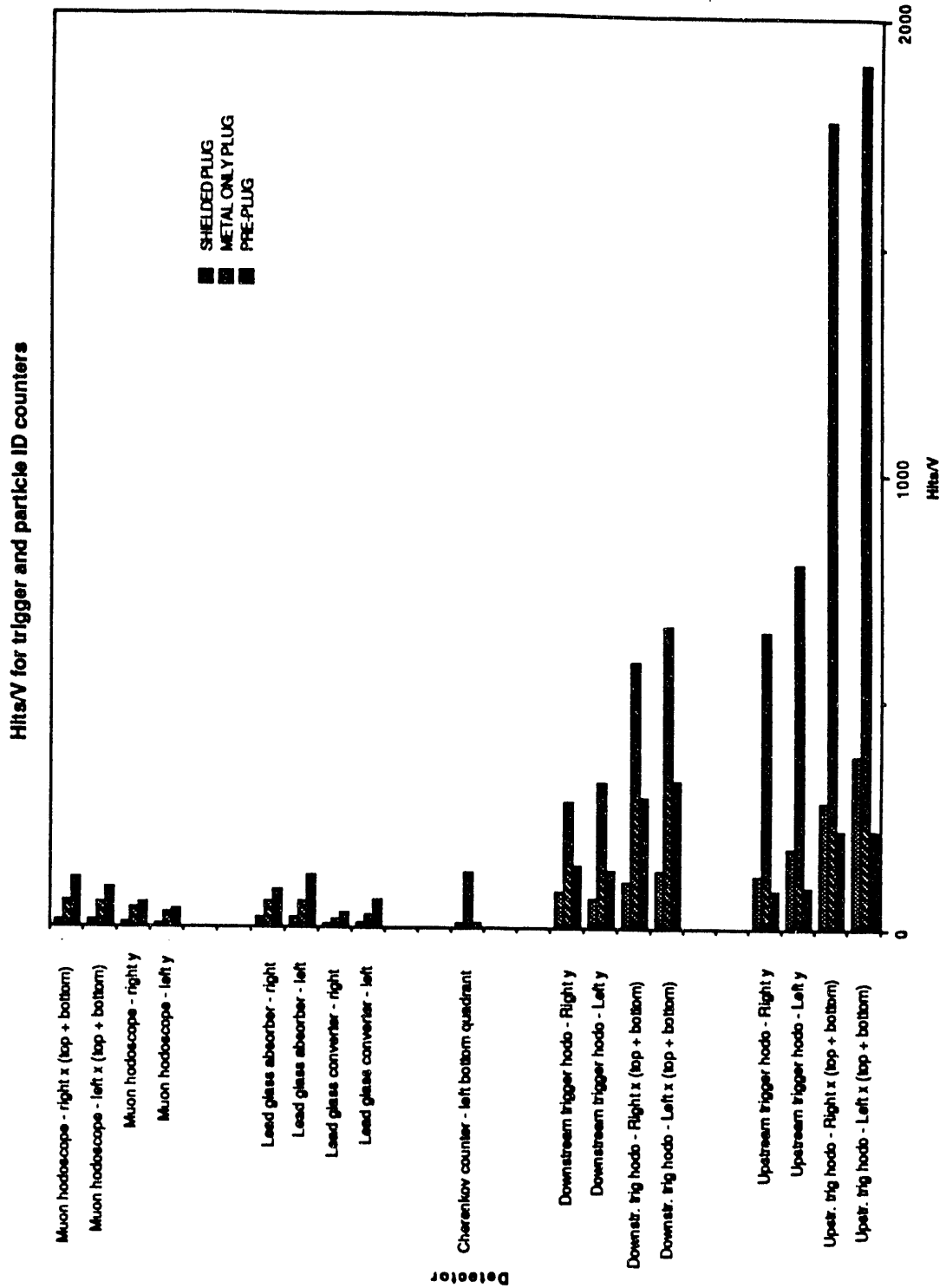
Figure 8: Trigger and particle identification detector rates in hits/V for three configurations of the plug.

Counter bank	Shielded plug at 15 Tp Single channel rate (KHz)	E791 at 4.5 Tp Single channel rate (KHz)
Upstream trigger counter	1,280*	192
Downstream trigger counter	494	298
Čerenkov counter	1,030**	253
PbG converter blocks	111	232
PbG back blocks	65	128
Muon hodoscope counters	209	304
* - In E871, this hodoscope will be farther from the plug.		
** - This does not include the reduction ($\simeq 2/3$) that can be made in the plug induced rate by locally shielding the phototubes.		

Table 4: Average single channel rates for E791 trigger counters and particle identification detectors for the shielded plug configuration, scaled to a proton beam intensity of 15 Tp/spill. The comparable rates are given for E791 at the beam intensity at which physics data were taken.

The lead glass and muon hodoscope rates in the plug geometry are considerably suppressed compared to the no plug case.

3.5 Test Run Summary

Measurements have been made that show that detector rates, though high in the region near the plug, ought to be manageable. At the outset of this effort, most of the concern was over neutrons from the plug interacting in chambers. Our plug design has succeeded in addressing this problem. While we have not yet achieved a fully satisfactory understanding of the plug and the sources of the detector rates, efforts to do so will continue. In fact, during the 1992 AGS run, further plug tests were conducted. It is possible, and perhaps likely, that as studies continue significant improvements can be made.

4 BNL Expt. 888

The E871 collaboration has been joined by physicists from Princeton, UCLA, and BNL to conduct a search at the AGS, using the E791 spectrometer, for an H dibaryon. Data taking is underway as this report is being written. The H is a hypothetical six-quark ($uuddss$) state. The E888 experiment consists of two distinct searches for the H. One uses the E791 spectrometer to look for single $\Lambda \to p\pi^-$ decays in the neutral beam in the vacuum decay region. These Λ's could come from H decays such as $H \to \Lambda n$. This search method is sensitive to H's with lifetimes in the range of 10^{-7} to 10^{-9} seconds. The second search involves significant rearrangement of the E791 spectrometer and looks for H interactions which produce two Λ's through diffractive dissociation in an active (scintillator) "dissociator" placed in the neutral beam. This method is sensitive to H lifetimes above 10^{-8}. Results from this experiment are expected to be available in the next six to nine months.

5 SSC Activities

Within the last year, a new collaboration has formed to construct a major detector to the SSC Laboratory. Known by the name GEM (Gammas, Electrons, and Muons), the principal goals of the detector are to emphasize precise measurment of photons, electrons,

34

and muons in SSC interactions. UT Austin has been a member of this collaboration from the beginning. Effort has centered in the general area of electronics, with emphasis on triggering and data acquisition. The major effort to date has been Monte Carlo simulation leading to an understanding of trigger rates, definition of trigger strategies, and preliminary specification of the trigger and data acquisition architecture, as described in various GEM documents (e.g., GEM Letter of Intent (SSCL-SR-1184), GEM Expression of Interest (SSC EOI-0020), GEM Baseline (GEM GDT-000015), GEM Baseline 1 (GEM TN-92-76) and others). Work is now underway to prepare the GEM Technical Design Report.

References

[1] R. D. Cousins et al., Phys. Rev. D **38**, 2914(1988).

[2] C. Mathiazhagan et al., Phys. Rev. Lett. **63**, 2181(1989).

[3] R. D. Cousins, C. Friedman, and P. L. Melese, IEEE Trans. in Nucl. Science **36**, 646(1989).

[4] K. A. Biery, D. A. Ouimette, and J. L. Ritchie, IEEE Trans. in Nucl. Science **36**, 650(1989).

[5] R. D. Cousins et al., Nucl. Instr. and Meth. **A277**, 517(1989).

[6] C. Mathiazhagan et al., Phys. Rev. Lett. **63**, 2185(1989).

[7] A. P. Heinson et al., Phys. Rev. **D44**, 44(1991).

[8] J. L. Ritchie, invited talk at the Topical Conference of the SLAC Summer Institute, July, 1990; W. R. Molzon, invited talk at TRIUMPF workshop, UCI90-52, July, 1990; W. R. Molzon, invited talk at the XXV International Conference on High Energy Physics, Singapore, August, 1990; A. Schwartz, invited talk at the 4th Conference on the Intersections between Particle and Nuclear Physics; Tucson, Arizona; May, 1991; S. Kettell, invited talk at the Vancouver DPF Meeting, August, 1991.

RECENT PUBLICATIONS

1. "Search for the Decays $K_L \to \mu e$ and $K_L \to ee$," R. D. Cousins $et\ al.$ (E791 collaboration), Phys. Rev. D **38**, 2914(1988).

2. "A Fast Integrating 8-bit Bilinear ADC," K. A. Biery, D. A. Ouimette, and J. L. Ritchie, IEEE Trans. on Nucl. Science, **36** 650(1989).

3. "Fast Parallel Pipelined Readout Architecture for a Completely Flash Digitizing System with Multilevel Trigger," R. D. Cousins $et\ al.$, Nucl. Instr. and Meth. **A277**, 517(1989).

4. "Lepton Flavor Violation in Rare Kaon Decays", by Jack L. Ritchie, Proceedings of the International Conference on CP Violation in Particle Physics and Astrophysics; Blois, France (May 1989), p. 511.

5. "CP Violation at the Main Injector: Report of the Working Group on CP Violation Experiments", J. L. Ritchie $et\ al.$, Proceedings of the Workshop on Physics at the Main Injector; Fermilab (May 1989), p. 85.

6. "Rare Kaon Decays", by Jack L. Ritchie, Proceedings of the Theoretical Advanced Study Institute in Elementary Particle Physics; Boulder, Colorado (June 1989), p. 711.

7. "New Experimental Limits on $K_L \to \mu e$ and $K_L \to ee$ Branching Ratios," C. Mathiazhagan $et\ al.$ (E791 collaboration), to Phys. Rev. Lett. **63**, 2181(1989).

8. "Measurement of the Branching Ratio for the Decay $K_L \to \mu\mu$", C. Mathiazhagan $et\ al.$, (E791 collaboration), Phys. Rev. Lett. **63**, 2185(1989).

9. "Higher Statistics Measurement of the Branching Ratio for the Decay $K_L \to \mu\mu$", A. P. Heinson $et\ al.$, (E791 collaboration), Phys. Rev. **D44**, 44(1991).

Progress Report

of

Task C

Experimental

1   Task C:

Outstanding Junior Investigator
Award for Dr. K.Lang
Progress Report 1991-1992

1.1   Introduction

Dr. Lang was selected for the Outstanding Junior Investigator Award in 1991 in response
to the proposal "Search for Very Rare Kaon Decays".

As the major activity on the BNL's AGS experiment E871 Dr. Lang has undertaken a
leading role in development and design of the tracking chambers based on drift straw tubes.
This project has been the central focus of dr. Lang's research in 1991-1992.

The main thrust of recent activities will be briefly reported in the following sections.

1.2   Outline of Activities

The experimental high energy physics group at the University of Texas has been founded
only recently with Dr. J.L. Ritchie as the first faculty hired in 1989, and Dr. Lang as the
second faculty hired in 1991.

As is typical of any new initiative the group had to invest a lot of time and effort to
setup laboratories in order to establish a sufficient basis for experimental work. With great
satisfaction we can report now that we have succeeded in setting up the working environment
capable to provide a high quality detector and software R&D.

Dr. Lang's research has focused on planning and design of the upstream tracking cham-
bers for the newly approved experiment E871 at BNL's Alternating Gradient Synchrotron.
The initial work has been oriented towards the following goals:

- furnish the lab with necessary equipment;

- gain hands-on experience with drift straw tubes and train personnel;

- present initial solutions to mechanical and electrical design issues related to: endplate
  geometry and mechanics, endplug and wire pins mechanics, electronics interface, gas

system and other;

- design a small test chamber and perform thorough evaluation of its performance;

- construct ~30 channel chamber to be tested at BNL in the 1992 H/test run;

All of the above tasks have been realized to various degrees. In addition, several systems necessary for a long time operation have been established:

- data acquisition system;

- gas mixing system;

- straw chamber assembly station;

- cosmic ray telescope;

- CAD software for chamber design;

In the process towards gaining experience of operating a straw drift chamber we have also constructed:

- 10-straw 30 cm long prototype;

- 30-straw 1 m long prototype;

- wire tension monitor and post-amplifiers for straw signals;

1.3 Main Results

The main direction of our recent efforts beyond a construction of a straw chamber was a thorough study of its performance. Most of this work is still in an early stage with no final conclusions. The areas of main interest included:

- understanding of the long term effects of tensioning straws;

- stable electro-mechanical operation of 1m long straws for gas mixtures of interest; measurement of position resolutions and efficiencies of individual straws with cosmic rays for all the gas mixtures;
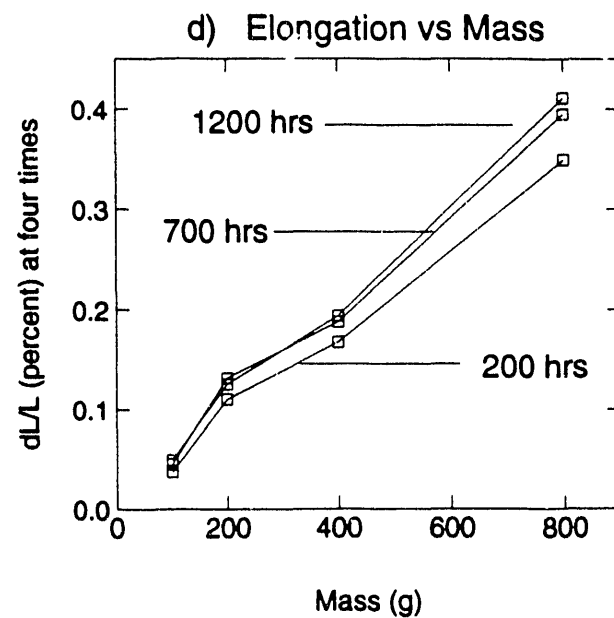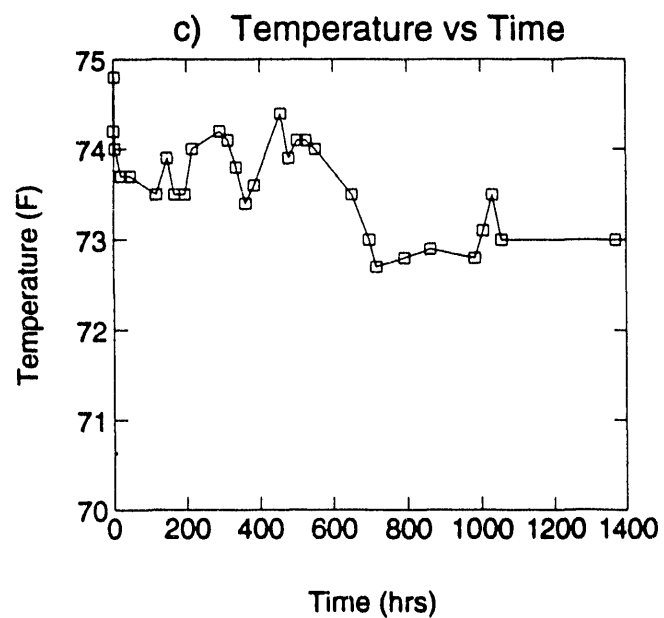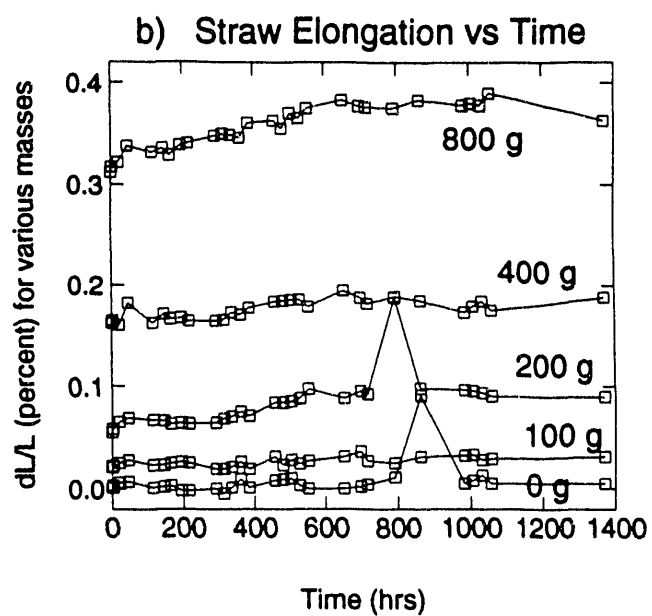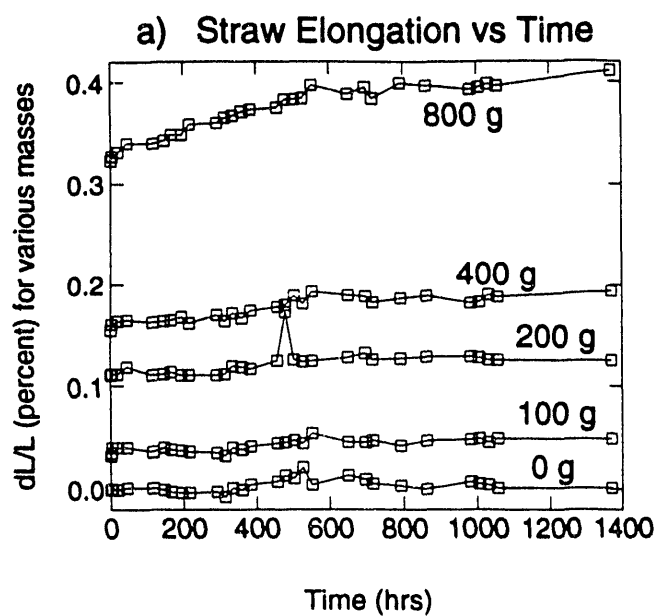
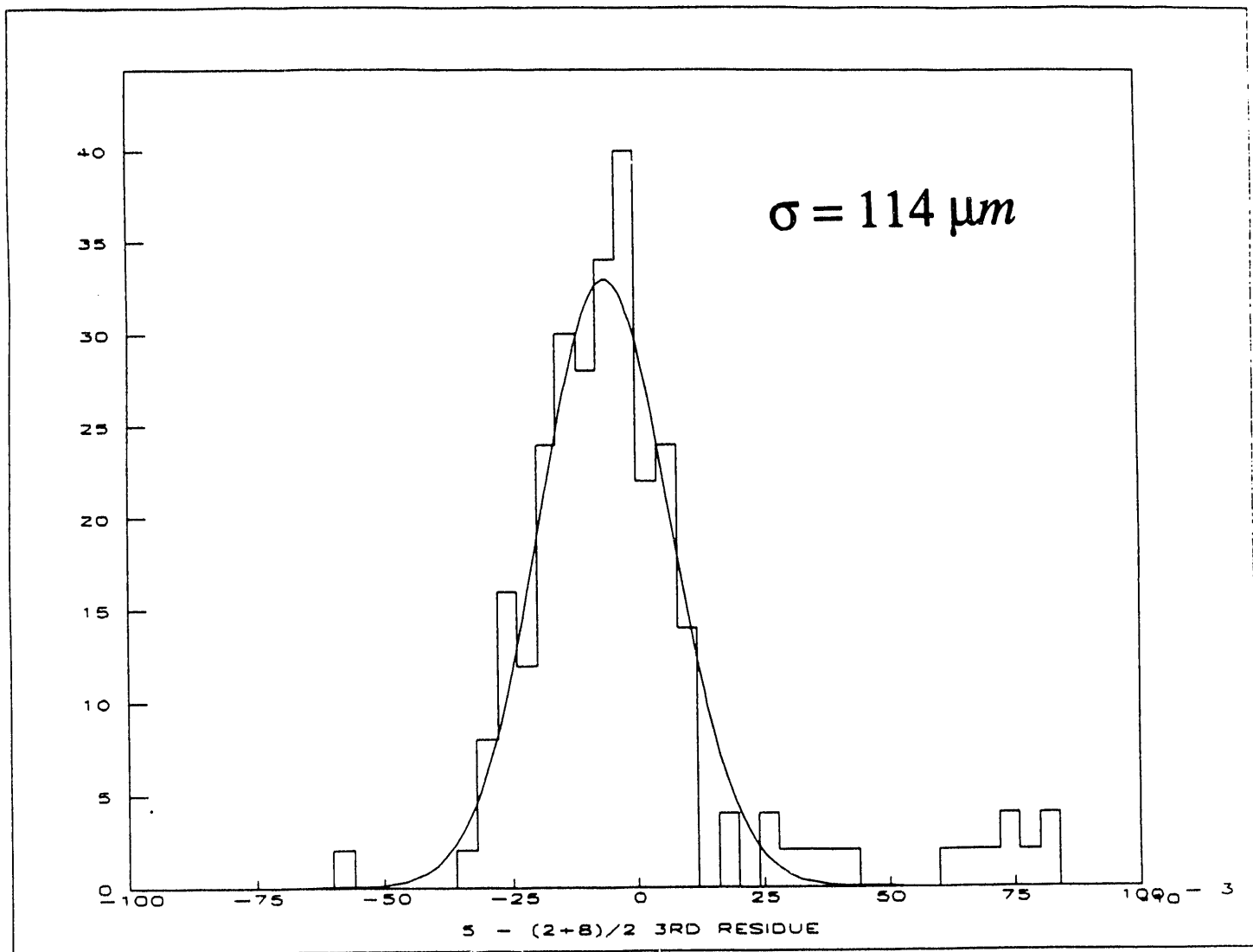Figure 1: Results of studies on straw elongation under a weight load.

Figure 2: Position resolution of 30 cm straws as measured for cosmic rays with argon-ethane gas mixture.

- measurement of rates, position resolutions and efficiencies of straws in the beam plug environment at BNL.

The final design of the straw drift chamber will take into account the results of studies underway. The issue of tensioning straws to assure a stable electro-mechanical operation touches upon a long term properties of straws under tension. We have initiated such study with a setup involving precision measurement of elongation of straws under weight loads. Figure 1 illustrates results of about 10 weeks of monitoring of straws under a weight loads indicating saturation of elongation for moderate loads.

Position resolutions and efficiencies are the two most critical parameters of straws. We plan to measure them for several gas mixtures with fast drift times (CF_4-ethane, CF_4-isobutane, CF_4-methane, and similar) and compare to argon-ethane, one of the standard mixture for drift chambers . At present time our preliminary results include resolutions and efficiencies for argon-ethane. Figure 2 displays a gaussian distribution of residuals of tracks of cosmic rays passing through a 30 cm long 10-straw test chamber. The best run so far has reached 105 μm resolution and 97.5% straw tube hit efficiency. We are currently working on measurements with fast gas mixtures.

The second prototype built has thirty 100 cm long straws arranged in a planar geometry similar to the planned for E871. After only a short checkout at UT the chamber was placed in the test beam at BNL as a part of 1992 series of E871 tests with the plug. Preliminary online measurements of rates give an optimistic view of straws operating close to the plug but results of these tests will be obtained in an offline analysis in the nearest future and are not available at this time.

1.4 Personnel

In December, 1991 our group was joined by a 3rd year full-time graduate student. His responsibilities focused on straw chamber related projects. As we move from the development stage to full size prototype stage the scope of the project escalates. For the summer 1992 we have hired two summer students to help in building a clean room and participate in tests.

1.5   Summary

The University of Texas group has started a program involving development and construction of the first two drift straw tube chambers for the AGS experiment E871. Present status of this project is still at the preliminary R&D stage and will evolve towards a full scale prototype production in the near future.

1.6 Recent Publications

1) **Measurement of the Branching Ratio** $K_L^0 \to \mu\mu$, C. Mathiazhagan *et. al.*, Phys. Rev. Lett. **63**:2183,1989.

2) **Measurement of the Proton Elastic Form-Factors for** $Q^2 = 1\text{-}3$ GeV/c^2, R.C. Walker *et al.*, Phys. Lett. **B224** (1989) 353-358.

3) **New Experimental Limits on** $K_L^0 \to \mu e$ **and** $K_L^0 \to ee$ **Branching Ratios**, C. Mathiazhagan *et. al.*, Phys.Rev.Lett. **63**:2185,1989.

4) **A Measurement of the Neutral Current Electroweak Parameters Using the Fermilab Narrow Band Neutrino Beam**, P. G. Reutens *et al.*, Z. Phys. **C45**:539-550,1990.

5) **Measurement of the Inclusive Charged Current Cross-section for Neutrino and Antineutrino Scattering on Isoscalar Nucleons**, P. S. Auchincloss *et al.*, Z.Phys. **C48**:411-432,1990.

6) **Higher Statistics Measurement of the Branching Ratio for the Decay** $K_L^0 \to \mu\mu$, A. P. Heinson *at al.*, Phys.Rev. **D44**:1-5,1991.

DATE
FILMED
12/28/92